encouraging outcomes, [12]. Even though recent studies have indicated that multi-stage electrode layouts may hold great promise for enhancing the effectiveness and efficacy of EHD devices, there hasn't been much experimental research on this subject.

The main goal of this work is to experimentally evaluate the performance of a prototype two-stage wire-to-mesh EHD air pump in a rectangular channel, under a positive corona discharge, which is a configuration that has not been studied in the bibliography. The good performance and minimal complexity of wire-to-plane arrangements, [3], provide easy construction and lower costs. The wire-to-mesh architecture is comparable to this particular setup since the plane collector has been replaced by a mesh made of multiple wires, which allows the air to flow through it, while at the same time keeping the electric field distribution almost similar to the wire-plate configuration, along the gap between the electrodes. On the other hand, positive corona discharge is used because it is highly stable and efficient, [13]. In the methodology section 2 that follows, the overall design and the experimental set-up of the prototype two-stage pump are presented, along with the circuit that supplies the device with high voltage. In section 3 the results of the obtained simulations for the optimization of the geometrical parameters of the prototypes and the experimental measurements are presented, along with the physical relationships that govern the phenomenon. Then a comparison is made between a single-stage and a two-stage EHD pump of similar size, showing the clear advantages of the two-stage configuration. Finally, in section 3.2 the two-stage prototype is compared with other mechanical fans or alternative EHD configurations found in the bibliography.

## 2 Methodology

The experimental two-stage EHD pump prototype that is presented in this work is constructed by cascading in series two wire emitter-mesh collector sets, each maintaining a constant potential difference between the corresponding emitter and collector. The emitter electrodes are made of a thin wire stretched across the opposite sides of a plexiglass rectangular channel. The collector electrodes are placed opposite to the corresponding emitters and consist of copper wires forming a rectangular mesh, as shown in Figure 1.

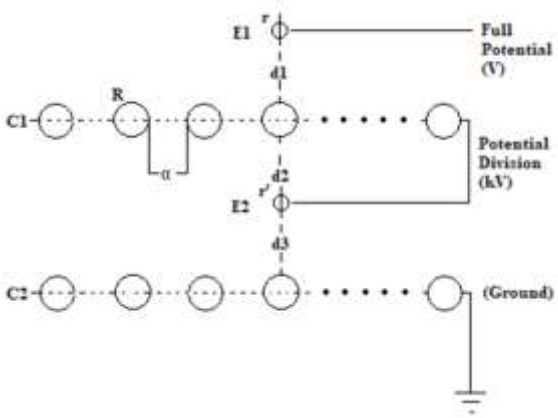


Fig. 1: Experimental configuration of two-stage EHD pump. E1 and E2 are the emitter electrodes, C1, C2 are the collector electrodes. The collector C1 and emitter E2 are equipotential (shorted) and are connected at the output of a high voltage divider with input high DC voltage V so that C1 and E2 are held at potential k.V, k being the division ratio of the divider.

Parallel wires have been used instead of dense mesh to minimize pressure drop at collectors C1 and C2. A software simulation based on Finite Element Analysis (FEA) has been conducted to optimize the final geometrical dimensions of the EHD pump prototype, assuming a distance of d=2 cm between the two stages. The FEA analysis has been carried out by using FEMM software, [24], to optimize cross-sectional radii r, r` of the emitters and the emitter-mesh gaps $d_1$, $d_2$, to achieve maximum electric field intensity along the emitter-collector gaps, for a given applied voltage V, as well as maximum electric field volume energy density around the electrodes, since the electric field is the determining factor for the generation of ionic wind, [2], [3], [15]. FEMM is a free electrostatic problems solver, which has been used in previous works, [4], [18], [20], and is based on well-known electric field laws, to calculate the electric field.

The differential form of Gauss' Law, defines that the flux out of any closed volume is equal to the charge contained within the volume

$$\nabla \cdot D = \rho \quad (1)$$

where ρ represents charge density.

Secondly, the differential form of Ampere's law

$$\nabla \times E = 0 \quad (2)$$

Displacement and field intensity are also related to one another via the constitutive relationship

$$D = \varepsilon E \quad (3)$$

where ε is the electrical permittivity of the medium where the electric field is applied.

The software employs the scalar potential V distribution in space, which is related to the electric field intensity according to the formula:

$$E = -\nabla V \quad (4)$$

Since the vector identity $\nabla\times\nabla\psi = 0$ is valid for any scalar ψ, Ampere's loop law (2) is automatically satisfied. Substituting into Gauss' Law and applying the constitutive relationship yields the second-order partial differential equation

$$-\varepsilon \nabla^2 V = \rho \quad (5)$$

which applies over regions of homogeneous ε.

FEMM solves (5) for voltage V over a user-defined domain with user-defined Dirichlet boundary conditions, [24]. Typical boundary conditions in this work have been the experimentally controlled constant voltage values at the electrodes of the EHD pump configuration.

The prototype pump has been subsequently built and tested, to experimentally evaluate its overall performance [24].

### 2.1 Experimental Setup

The necessary high voltage has been provided by a Matsusada Precision W series variable High-Voltage 0-40kV generator. A high-voltage shielded DC cable, supplies the EHD pump for the generation of the electrical wind flow, after the onset of the corona discharge current. To ensure that each stage of the two-stage pump receives the necessary fraction of the total voltage V a high voltage divider has been used. High voltage measurements on the prototype pump have been performed with an accuracy of 1% by using a Peak Tech 2010 DMM multimeter along with a Coline HV40B 1000:1 high-voltage probe. A Thurlby 1503 microammeter with a sensitivity of 1nA has been used to acquire corona current measurements. To measure the generated airspeed, a Testo 405 hot wire anemometer (5% accuracy) has been installed at a 2 cm distance from the grounded collector C2 at the pump's output. Figure 2 shows the experimental setup that has been used to evaluate the pump prototype. Regarding the rectangular channel dimensions, the flow cross section is 5cm high and 10cm wide and the overall channel length is 20cm.

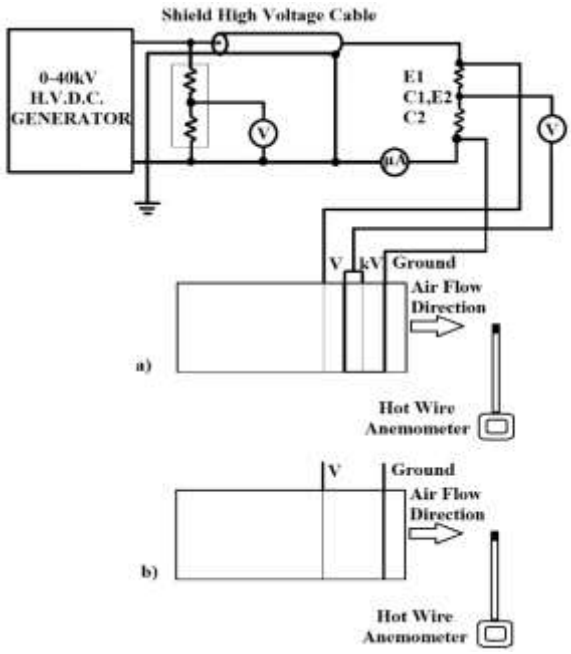


Fig. 2: a) Measurement equipment configuration and experimental set-up for two-stage EHD pump, b) single-stage configuration. The rectangular channel outer limits are also shown.

## 3 Results and discussion

According to the optimization process carried out by the FEMM software to determine the required geometrical characteristics of the presented EHD pump configuration electrodes, a constant distance of d=2cm and various Ni-Cr wire combinations for the construction of emitters and collectors have been examined. The resulting optimized geometric configurations for the single-stage and two-stage prototypes are given in Table 1 and Table 2, respectively. These configurations ensure maximum electric field intensity in the vicinity of the emitters while, at the same time, retaining high spatial energy density between the emitter-collector electrodes for a given applied voltage difference. It should be noted that in the two-stage configuration, the high voltage division ratio k, according to Figure 1, is quite important. For example, supposing that both emitters have identical cross-sections (r=r`) a division ratio of k=0.5 divides equally the total applied voltage V between the two stages, but then the electric field strength around emitter E2 is expected to be lower than the corresponding electric field strength around emitter E1, due to the deformation of the electric field caused by collector C1 which is shorted with

E2, as shown in Figure 1. To ensure that both stages reach the threshold field for air-ionization simultaneously, thus maximizing electric wind flow, a suitable combination of electrode geometry parameters and a suitable potential division ratio k is required. As shown in Table 2, in this study a combination of k=0.5 with different wire selections for E1 and E2 construction, with r=90 μm and r`=30 μm, ensures that the electric field strength in the vicinity of both emitters reaches almost identical values, for a given applied potential V. This has been verified by FEMM simulations, with a fine 10 μm mesh and a maximum simulation error of $1.e^{-008}$. This number specifies the stopping criterion for the linear solver [24].

**TABLE 1**
**DETAILS OF SINGLE STAGE EHD PROTOTYPE**

| *a (mm)* | *r (μm)* | *R (μm)* | *d(mm)* |
|---|---|---|---|
| *10* | *90* | *300* | *60* |
| *Final configuration details* | | | |
| *E: 1 wire with 90μm radius* | | | |
| *C: 11 wires with 300μm radius each* | | | |

**TABLE 2**
**DETAILS FOR TWO-STAGE EHD PROTOTYPE**

| *a (mm)* | *r (μm)* | *r' (μm)* | *R (μm)* | *d (mm)* |
|---|---|---|---|---|
| *10* | *90* | *30* | *300* | *20* |
| *Final configuration details* | | | | |
| *E1: 1 wire with 90 μm radius* | | | | |
| *E2: 1 wire with 30μm radius* | | | | |
| *C1: 11 wires with 300 μm radius each* | | | | |
| *C2: 11 wires with 300 μm radius each* | | | | |

The electrical field intensity (E) and voltage (V) distribution along the airflow axis, have been plotted on a fine step of 10μm from simulations. This is shown in Figure 3 for the two-stage configuration according to Table 2. In addition, similar curves for the single-stage EHD pump prototype of Table 1 are given in Figure 4.

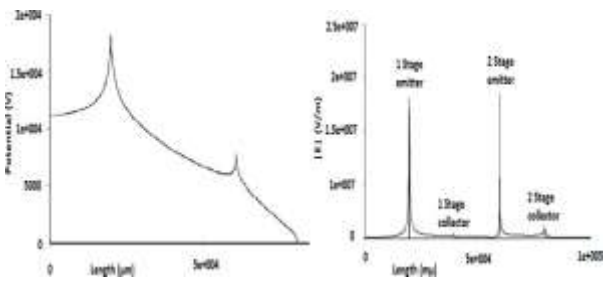

Fig. 3: The distribution V along the airflow axis for the applied voltage of 17 kV across E1 and C1, while E2 and C2 are kept at 8.5 kV (k=0.5).

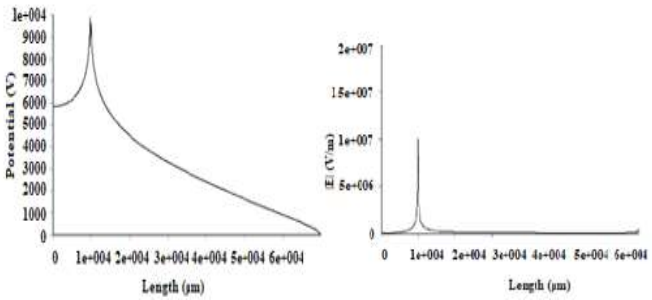


Fig. 4: FEMM results for the single-stage EHD pump for a voltage difference V of 10kV between the emitter and collector.

Figure 5 shows the potential distribution in the space between the electrodes in both the first and second stages. The areas with red color have with highest levels of potential in contrast to areas of light blue color the level of the potential in the space is at zero levels. Accordingly, Figure 6 shows the distribution of the electric field. The value of the electric field strength at emitter E1 is $1.92x10^7$ V/m, while the corresponding value at emitter E2 is $1.82x10^7$ V/m.

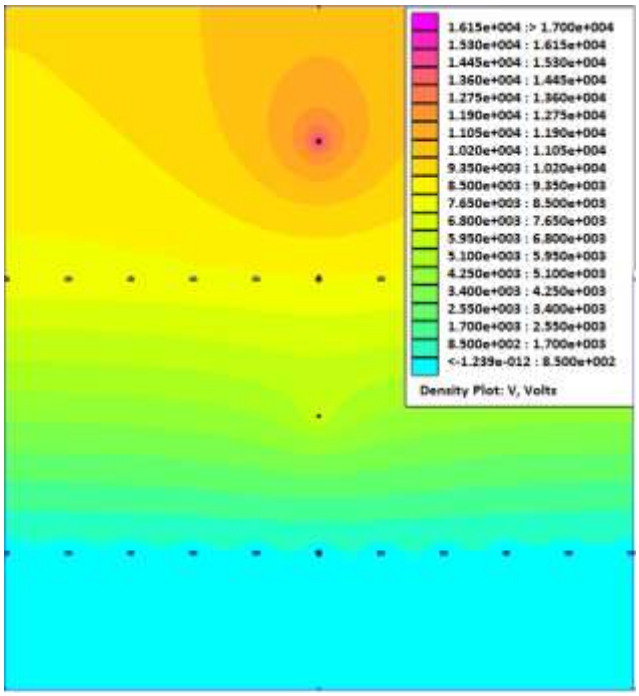


Fig. 5: FEMM results for the electric potential distribution in a two-stage configuration.

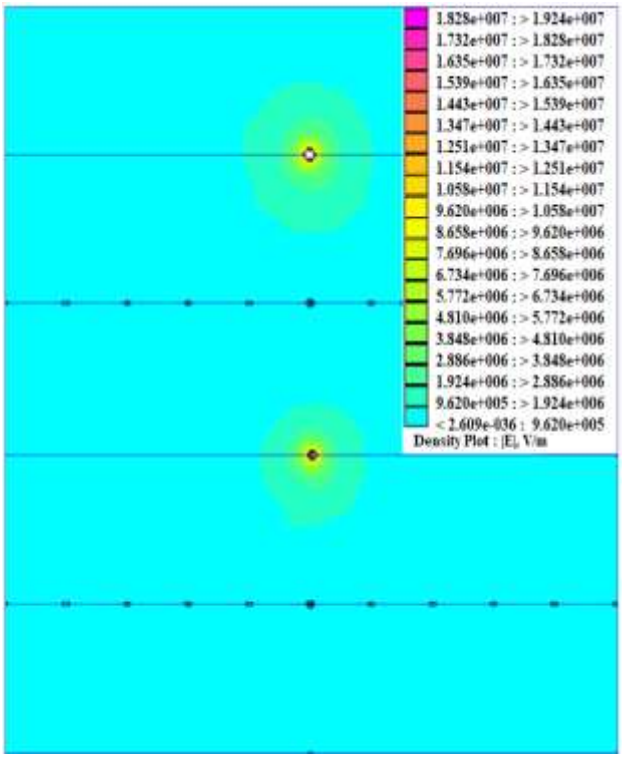

Fig. 6: FEMM results for the electric field strength distribution in a two-stage EHD pump.

### 3.1 Experimental Evaluation Results

The experimental setup shown in Figure 2 has been used to evaluate the constructed EHD pump prototypes in terms of the generated air velocity *v (m/s)* at various voltage levels *V (kV)*. The total current flow *I(μA)* that is provided to the EHD pump was also recorded. Throughout the experiments, the room temperature averaged 24,3 °C, ranging from 19,6°C to 29,1°C. The relative humidity (RH) averaged 43,6% ranging from 35,2% to 52,1%. In terms of breakdown voltage, the two-stage arrangement waslimited to 41 kV, which was the real measured maximum output of the high-voltage generator, slightly above the 40 kV maximum output rating provided by the generator specs.

The electric power consumption by the EHD prototypes $P_E$ *(W)* has been calculated as:

$$P_E = I \cdot V \quad (6)$$

The mechanical output power $P_W$ of the generated airflow has been calculated as:

$$P_W = {}^1/_2 \cdot A \cdot \rho \cdot v^3 \quad (7)$$

where *A(m)* is the rectangular channel's cross-section, $\rho$ is the air density (1,17 kg/m$^3$ at 29 °C) and *v (m/s)* is the wind velocity.

Finally, the EHD pump's overall efficiency, n, is calculated with the ratio

$$n = P_W / P_E \quad (8)$$

When ionized air molecules drift toward the collector, corona discharges occur in the vicinity of the emitter. Corona current is defined by Townsend's, [1], formula:

$$I = k \cdot (V - V_0)^2 \quad (9)$$

where *I* is the corona discharge current in $\mu A$, *V* is the applied voltage in *kV*, *Vo* is the ionization inception voltage in *kV* and *k* represents a constant term in $\mu A/kV^2$. According to the literature, *k* depends on several variables, including electrode separation distance, emitter and collector radius, ion mobility, and dielectric permittivity, [1]. In this case, *k* increases also with collector radius, and *k* and *Vo* values, as given in Table 3 have been determined by a least square fitting method on the current experimental results. The study, [14], found through a parametric study that the speed of the airflow is a function of the square root of the Corona current multiplied by an empirical constant term, according to the expression:

$$v = K \cdot \sqrt{I} \quad (10)$$

where *v (m/s)* is the wind velocity, *I (μA)* is the Corona current in $\mu A$ and *K* is a constant term. The experimental results for the corona current in the single-stage configuration are given in Figure 7.

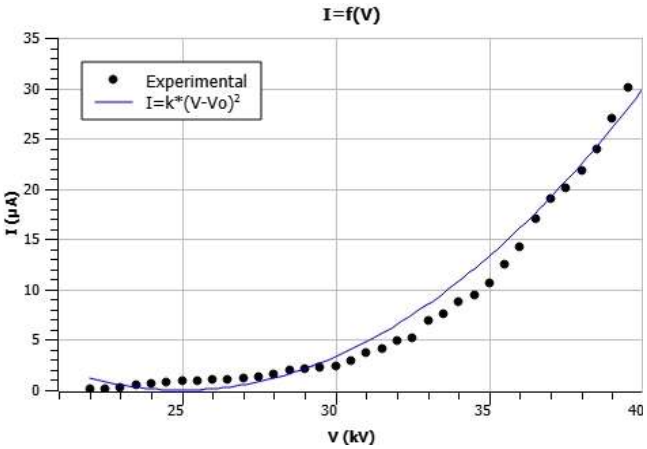

Fig. 7: Experimental and theoretical corona discharge current with the applied voltage in the single-stage EHD pump prototype with r=90m, R=300μm, a=1cm, and d=6cm.

The results for the two-stage configuration are shown in Figure 8.

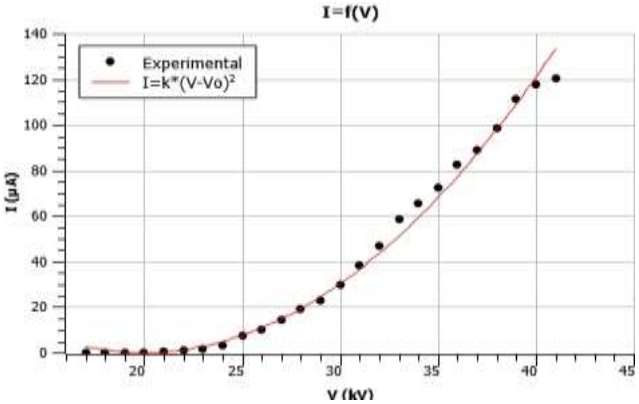


Fig. 8: Two-stage pump experimental and theoretical curve of corona current variation with the applied potential difference, where the geometrical parameters of the pump prototype are *r=90μm, r'=30μm, R=300μm, a=1cm, d1=d2=d3=2cm.*

Table 3 shows ionization inception voltage $V_0$ with collector radius *R* and emitter radius *r*, and the constant *k*, according to equation (9), which equals *0.13* for the two-stage EHD configuration and *0.30* for the single-stage configuration, both of identical overall length *d=6cm*, to obtain comparable results.

TABLE 3
TERMS FOR THE CORONA DISHCHARGE CURRENT EQUATIONS

| *Emitter radius r [μm]* | *Collector radius R [μm]* | *Constant term k [μA/kV²]* | *Inception Voltage Vo [kV]* | *Breakdown Voltage V [kV]* |
|---|---|---|---|---|
| *90-30* | *300* | *0,13* | *17* | *41* |
| *30* | *300* | *0,30* | *22* | *40* |
| *90* | | | | |

Fitting curves were drawn according to equation (9) and the fit was very close. The inception voltage was *17kV* for the two-stage configuration and *22kV* for the single-stage configuration. In Figure 9 the variation of air flow velocity *v* in relation to the corona discharge current *I* is shown. The experimental measurements were acquired from the two-stage configuration and a comparison was made with the theoretical curve, obtained from the equation (10).

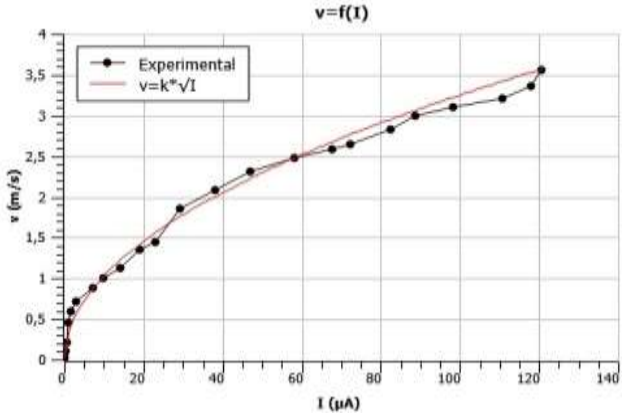


Fig. 9: Two-stage EHD pump experimental measurements *v=f(I).*

The constant term *K* for the theoretical curve of wind velocity, according to equation (10) was *0.24*. Also, the change of ionic wind velocity *v* with applied voltage *V* has been examined, with the results shown in Figure 10 for both EHD pump prototypes.

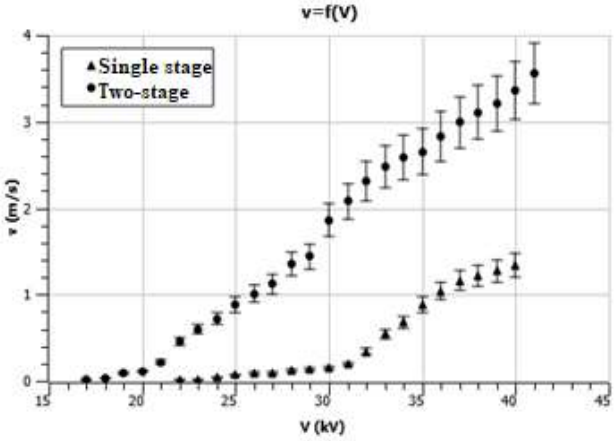


Fig. 10: EHD air velocity with voltage, on both single-stage and two-stage EHD pumps.

In Figure 10 becomes clear the difference in the ionization inception voltage between the single-stage and two-stage prototypes, which is approximately 22%. The two-stage pump produces significantly higher air velocity at the same voltage level than the single stage, which is a clear advantage.

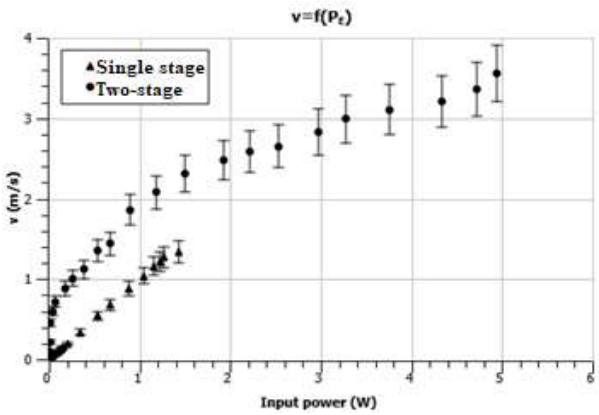


Fig. 11: EHD air velocity *v* variation with electrical input power according to equation (6).

This is consistent with the air velocity results according to the input power usage, as given in Figure 11. It is clear that for the same overall dimensions, the two-stage EHD pump is more efficient than the single-stage EHD pump. Moreover, the operation of the single-stage configuration is unstable because there is an increased risk of undesirable breakdowns. Additionally, the results for the pump efficiency *n*, as calculated by applying equation (8) to the experimental data, are given in Figure 12. Accordingly, the efficiency of the two-stage EHD pump did not exceed 4.48%, while the single-stage pump corresponding value had been 0.65%, which shows the advantage of the two-stage configuration.

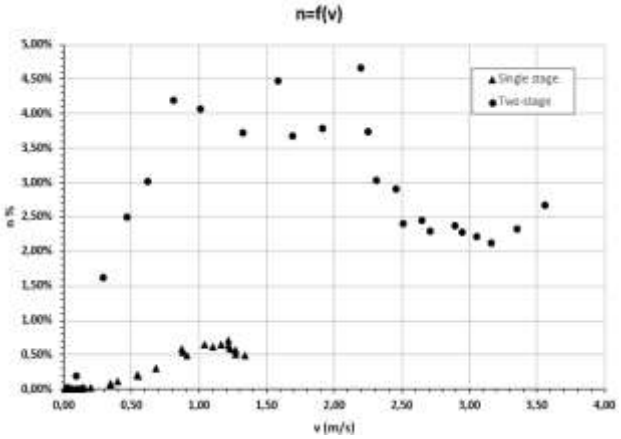


Fig. 12: Efficiency to air-velocity variation.

### 3.2 Mechanical Fans and other EHD Configurations Compared with the Prototype Two-Stage EHD Pump

A consequence of the operation of electronic components is the generation of heat. This heat must be reduced in intensity or transferred to the environment, outside the device. In this case, the most widely applied solution for cooling applications is the choice of mechanical fans. Some advantages and disadvantages characterize this selection. A big disadvantage is the operating noise, the large air outlet surface, and the limitations in the design when they have to be placed in narrow spaces as in laptops, where a quiet operation is also required. Other disadvantages are the presence of moving parts, which require lubrication, and the production of additional heat generated by the operation of the moving parts. Advantages include low operating voltage typically 12v and high air speeds. EHD pumps also function as thrusters in space applications. Besides, EHD has become a well-established technology in propulsion devices for small satellites, such as CubeSats, [16], or food drying, [17].

An overall comparison of the presented two-stage EHD pump prototype with other high-quality mechanical fans or alternative EHD configurations found in the bibliography is given in Table 4.

The mechanical fans shown in the table are of similar dimensions, with a diameter ranging from 80mm to 120 mm. The experimental results have shown that in fact, the prototype is capable of directly competing with mechanical fans in free air while providing comparable energy efficiency and virtually zero noise, which is an important aspect for certain, applications.

## 4 Conclusion

Finite element analysis simulations have been used to optimize the geometrical characteristics and, consequently, the overall efficiency of a two-stage wire-to-mesh EHD air pump, where the two stages are cascaded in a series configuration. Since the electric field is the governing factor determining the produced air wind flow between the electrodes of the EHD two-stage pump, an effort has been made to maximize the electric field strength by proper design of the electrodes, while at the same time, maintaining the applied high voltage at the lowest possible value.

TABLE 4

THE PROPOSED TWO-STAGE EHD PROTOTYPE COMPARED WITH HIGH QUALITY COMMERCIAL MECHANICAL FANS AND OTHER EHD AIR PUMP CONFIGURATIONS

| Device type Author(s) | Acoustic Noise (dBA) | Maximum Air Velocity v (m/s) | CFM | Power $P_E$ (W) | Rotational Speed (RPM) | Air velocity Outlet Surface $(mm)^2$ | Operating Voltage (V) | Current (A) |
|---|---|---|---|---|---|---|---|---|
| Noctua NF-S 12B, [15]. Redux | 18.1 | 3.45 | 59.2 | 1 | 1200 | 11304 | 12 | 0.08 |
| Corsair QL-120, [15]. | 26 | 2.43 | 42.8 | 3.96 | 1500 | 11304 | 6-13.2 | 0.3 |
| Noctua NF-A8 ULN, [15]. | 10.5 | 1.92 | 20.5 | 0.6 | 1400 | 5024 | 12 | 0.05 |
| S. Tampouris *et al.* Present Study | (*) | 3.56 | 61.16 | 4.48 | (-) | 5000 | $41 \cdot 10^3$ | $1.2 \cdot 10^{-4}$ |
| E. Fylladitakis *et al.* [4]. | (*) | 1.77 | 42.4 | 7.35 | (-) | 11304 | $21 \cdot 10^3$ | $3.5 \cdot 10^{-4}$ |
| S. Sumariyah et al. [19]. | (*) | 1 | 3.83 | 0.1 | (-) | 452 | $3.8 \cdot 10^3$ | $2 \cdot 10^{-4}$ |
| J.H. Lin et al. [21]. | (*) | 2.2 | 12.03 | 1.02 | (-) | 3000 | $17 \cdot 10^3$ | $6 \cdot 10^{-5}$ |
| E. Fylladitakis et al. [18]. | (*) | 1.47 | 24.42 | 0.62 | (-) | 7854 | $25 \cdot 10^3$ | $2.2 \cdot 10^{-5}$ |
| H. Tsubone et al. [23]. | (*) | 2.23 | 2.64 | 1.44 | (-) | 560 | $10 \cdot 10^3$ | $14 \cdot 10^{-4}$ |
| E. Calvo et al. [22]. | (*) | 0.52 | 1.99 | 3.2 | (-) | 452 | $40 \cdot 10^3$ | $8 \cdot 10^{-5}$ |

(*) The created noise is so low that it hardly distinguishes from the surrounding noise.
(-) There is not rotational speed, no moving parts.

The presented two-stage prototype has been experimentally tested in comparison with a single-stage prototype of equal length. The results have shown the clear advantages of the two-stage configuration over the single-stage configuration, in terms of the lower required threshold voltage for air-wind onset, and the higher air flow velocity and higher overall efficiency as a ratio of the net mechanical flow power output to the required electrical power input.

It has been also shown that in a direct comparison with commercial fans of similar dimensions or other EHD pump configurations found in the bibliography, the proposed prototype two-stage pump is quite competitive.

*References:*

[1] J. S. E. Townsend, *Electricity in gases*. Oxford: Clarendon Press,1915.

[2] L. B. Loeb, *Electrical coronas*. London: University of California Press, 1965.

[3] E. D. Fylladitakis, M. P. Theodoridis, and A. X. Moronis, "Review on the History, Research, and Applications of Electrohydrodynamics," *Plasma Science, IEEE Transactions on*, Vol. 42, 2014, pp. 358-375.

[4] E. D. Fylladitakis, A. X. Moronis, and K. N. Kiousis, "Evaluation of a single needle to grid EHD pump prototype for forced convection cooling applications," presented at the *International Conference on Energy, Environment, Ecosystems and Development*. (EEED 2013), Rhodes Island, Greece, 2013.

[5] Q. Wei, X. Lingzhi, Y. Lanjun, Z. Qiaogen, X. Lei, and C. Li, "Experimental Study on the Velocity and Efficiency Characteristics of a Serial Staged Needle Array-Mesh Type EHD Gas Pump," *Plasma Science and Technology*, Vol. 13, 2011, pp. 693-694.

[6] A. A. Martins, "Simulation of a wire-cylinder-plate positive corona discharge in nitrogen gas at atmospheric pressure," *Physics of Plasmas*, Vol. 19, 2012, pp. 63-64-65.

[7] J.-D. Moon, D.-h. Hwang, and S.-T. Geum, "An EHD gas pump utilizing a ring/needle electrode," *IEEE Transactions on Dielectrics and Electrical Insulation*, Vol. 16, 2009, pp. 352-358.

[8] J. M. Crowley, G. S. Wright, and J. C. Chato, "Selecting a working fluid to increase the efficiency and flow rate of an EHD pump," *Industry Applications, IEEE Transactions on*, Vol. 26, 1990, pp. 42-49.

[9] E. Moreau and G. Touchard, "Enhancing the

mechanical efficiency of electric wind in corona discharges," *Journal of Electrostatics*, Vol. 66, 2008, pp. 39-44.

[10] C. Kim, D. Park, K. C. Noh, and J. Hwang, "Velocity and energy conversion efficiency characteristics of ionic wind generator in a multistage configuration," *Journal of Electrostatics*, vol. 68, 2009, pp. 36-41.

[11] K.Masuyama, "*Performance characterization of electrohydrodynamic propulsion devices*," Master of Science Thesis, Department of Aeronautics and Astronautics, Massachusetts Institute of Technology, Massachusetts, USA, 2012

[12] W. Qiu, L. Xia, X. Tan, and L. Yang, "The Velocity Characteristics of a Serial-Staged EHD Gas Pump in Air," *Plasma Science, IEEE Transactions on*, Vol. 38, 2010, pp. 2848-2853.

[13] M. S. June, J. Kribs, and K. M. Lyons, "Measuring efficiency of positive and negative ionic wind devices for comparison to fans and blowers," *Journal of Electrostatics*, vol. 69, 2011, pp. 345-350.

[14] M. Robinson, " Convective heat transfer at the surface of a corona electrode", *Int J. Heat Mass Transf.*, Vol 13, No. 2, 1970, pp. 263-274

[15] Y. Peng, D. Li, X. Yang, Z. Ma, Z. Mao, A review on Electrohydrodynamic (EHD) pump, *Journal Micromachines*, Vol. 14, 2023, pp. 7-8.

[16] Levchenko, I.Bazaka, K. Belmonte, T. Keidar, M. Xu, Advanced Materials for Next-Generation Spacecraft, *Advance Materials*, Vol. 30, 2018, pp. 3-4.

[17] Amoasah, B., Appiah, F., Tandoh, P., & Amoateng, Effect of different drying methods on the mineral content of three accessions of Roselle (Hibiscus sabdariffa) calyces, *Asian Journal of Advanced Research and Reports*, Vol. 5, 2019, pp.7-9.

[18] A. Moronis, E. Fylladitakis, Experimental Evaluation on an Electrohydrodynamic CPU Cooling System Utilizing a Wire-Grid Electrode Configuration, *International Conference' Science in Technology',2015, pp.2-3.*

[19] S. Sumariah, K. Kusminarto, A. Hermanto, P. Nuswantoro, Study of EHD flow generator's efficiencies utilizing pin to single ring and multi-concentric rings electrodes, *8th International Conference on Physics and its Applications, 2016, pp.3-5.*

[20] A. Moronis, E. Fylladitakis, I. Raptis, Two-stage Cascaded EHD Air Pump Evaluation, *IEEE International Conference on High Voltage Engineering and Application, 2018, pp.2-4.*

[21] J.H.Lin, S.C.Lin, Feng Lai, Performance of an electrohydrodynamic gas pump fitted within a nozzle, *Journal of Electrostatics*, 2018, pp. 2-5.

[22] E. Calvo, M. Pinheiro, Modeling of Electrohydrodynamic (EHD) Plasma Thrusters Optimization of Physical and Geometrical Parameters, *Journal Applied Sciences*, 2022, pp. 1-3.

[23] H. Tsubone, Experimental and Analytical Investigation of Wire-Partially Insulated Parallel Plate Electrode Type Electrohydrodynamic Fan, *International Journal Machines*, Vol 11, 2023, pp.1-2.

[24] FEMM Documentation, Users Manual https://www.femm.info/Archives/doc/manual42.pdf, Dnld 2023, pp. 9-22 (Accessed Date: 02/10/2023).

**Contribution of Individual Authors to the Creation of a Scientific Article (Ghostwriting Policy)**

The authors equally contributed in the present research, at all stages from the formulation of the problem to the final findings and solution.

**Sources of Funding for Research Presented in a Scientific Article or Scientific Article Itself**

No funding was received for conducting this study.

**Conflict of Interest**

The authors have no conflict of interest to declare.